JACS
JOURNAL OF THE AMERICAN CHEMICAL SOCIETY
pubs.acs.org/JACS
Article

Adsorbed Enolate as the Precursor for the C−C Bond Splitting during Ethanol Electrooxidation on Pt

Hongsen Wang and Héctor D. Abruña*

Cite This: https://doi.org/10.1021/jacs.2c13401
Read Online

ABSTRACT: Ethanol is a promising alternative fuel to methanol for direct alcohol fuel cells. However, the complete electrooxidation of ethanol to CO_2 involves 12 electrons and C−C bond splitting so that the detailed mechanism of ethanol decomposition/oxidation remains elusive. In this work, a spectroscopic platform, combining SEIRA spectroscopy with DEMS, and isotopic labeling were employed to study ethanol electrooxidation on Pt under well-defined electrolyte flow conditions. Time- and potential-dependent SEIRA spectra and mass spectrometric signals of volatile species were simultaneously obtained. For the first time, adsorbed enolate was identified with SEIRA spectroscopy as the precursor for C−C bond splitting during ethanol oxidation on Pt. The C−C bond rupture of adsorbed enolate led to the formation of CO and CH_x ad-species. Adsorbed enolate can also be further oxidized to adsorbed ketene at higher potentials or reduced to vinyl/vinylidene ad-species in the hydrogen region. CH_x and vinyl/vinylidene ad-species can be reductively desorbed only at potentials below 0.2 and 0.1 V, respectively, or oxidized to CO_2 only at potentials above 0.8 V, and thus they poison Pt surfaces. These new mechanistic insights will help provide design criteria for higher-performing and more durable electrocatalysts for direct ethanol fuel cells.

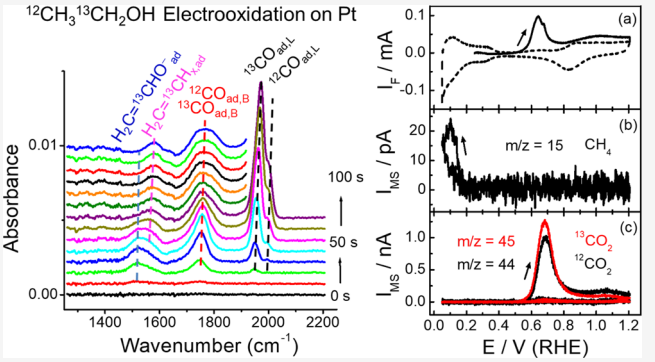

1. INTRODUCTION

Compared to internal combustion engines, fuel cells possess higher energy conversion efficiencies, and thus have attracted increasing attention. Among different types of fuel cells, hydrogen fuel cells have been extensively studied as potential power sources.[1−3] However, hydrogen gas has a very low volumetric energy density and is difficult to handle. Direct ethanol fuel cells (DEFCs) have advantages over hydrogen fuel cells.[4−6] Ethanol has a higher volumetric energy density than hydrogen and is a renewable fuel that can be generated from biomass or via the reduction of carbon dioxide.[7−9]

However, the complete electrooxidation of ethanol to CO_2 involves 12 electrons, and thus, a number of adsorbed and soluble intermediates are generated.[10−22] Among them, CO and other non-CO ad-species can adsorb onto Pt surfaces, and consequently poison Pt.[12−14,17,19,20,23−25] Ethanol electrooxidation on Pt-based catalysts mainly generates acetaldehyde and acetic acid, and the current efficiency (CE) for CO_2 generation is very low because C−C bond splitting and subsequent oxidation are slower than the oxidation reaction without C−C bond rupture.[10,22,23,25,26] Rh has been claimed to enhance C−C bond splitting in PtRh and Pt-Rh-SnO_2 catalysts, thus increasing CE for CO_2 formation.[27,28] However, DEMS measurements did not support such claims.[29,30] Although ethanol electrooxidation on Pt has been studied for decades, the mechanistic details of ethanol decomposition and oxidation still remain elusive.

In this work, we used a home-built spectroscopic platform, which combined surface-enhanced infrared absorption (SEIRA) spectroscopy with differential electrochemical mass spectrometry (DEMS) through a dual thin-layer spectroelectrochemical flow cell (Figure 1A). This enabled identification of surface adsorbed species during ethanol decomposition/electrooxidation on Pt using SEIRA spectroscopy, and simultaneous detection of volatile solution products by employing DEMS under well-defined flow conditions. Under the well-defined flow conditions of our cell design, the effects of ethanol depletion, which is well known to take place in the thin-layer external reflection configuration of infrared reflection absorption spectroscopy, as well as product readsorption, can be significantly mitigated. For the first time, adsorbed enolate has been identified as the precursor for the C−C bond splitting during ethanol electrooxidation on Pt, and a detailed ethanol decomposition/electrooxidation mechanism is proposed. The new insights into the ethanol electrooxidation mechanism will

Received: December 15, 2022

https://doi.org/10.1021/jacs.2c13401
J. Am. Chem. Soc. XXXX, XXX, XXX−XXX

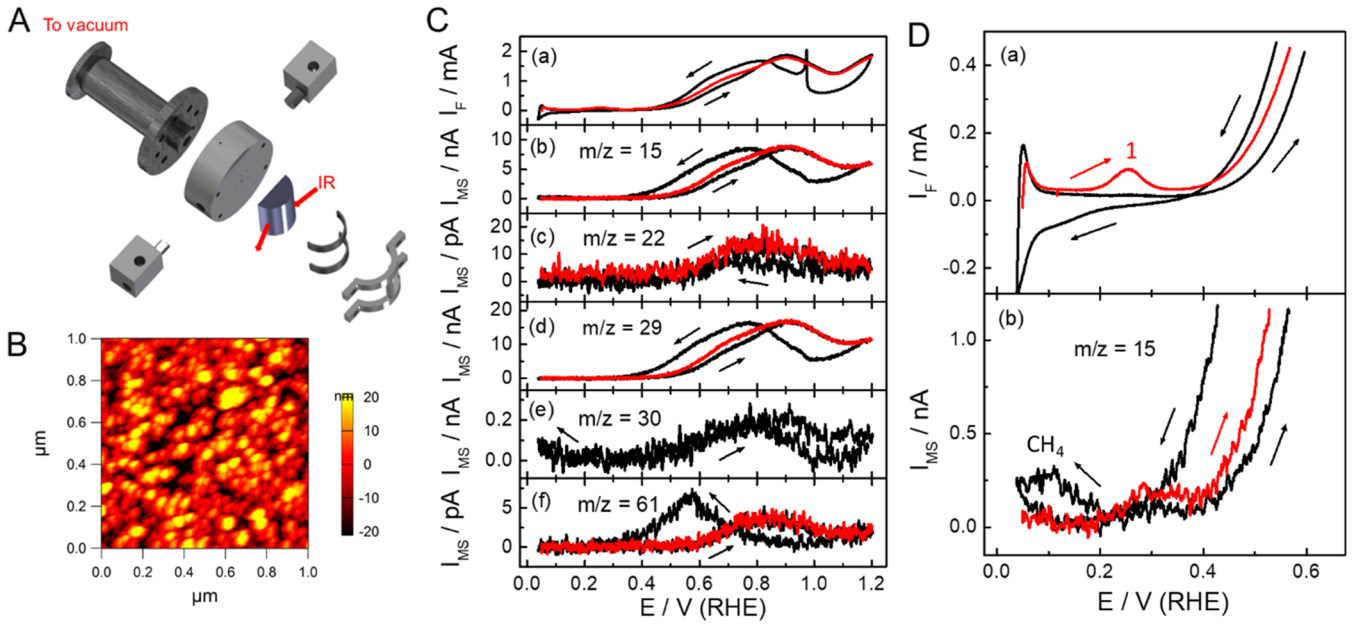

Figure 1. (A) Illustration of the dual thin-layer flow cell for simultaneous DEMS and FTIR investigations. (B) AFM image of Pt film chemically deposited on a Si prism. (C) Cyclic voltammograms for ethanol electrooxidation on a Pt film in 0.1 M ethanol + 0.1 M $HClO_4$ at a scan rate of 5 mV/s (a), and corresponding mass spectrometric signals at m/z = 15 (b), m/z = 22 (c), m/z = 29 (d), m/z = 30 (e), and m/z = 61 (f). The red traces show the first positive-going scan. (D) Expanded low-potential region of Figure 1C (a and b).

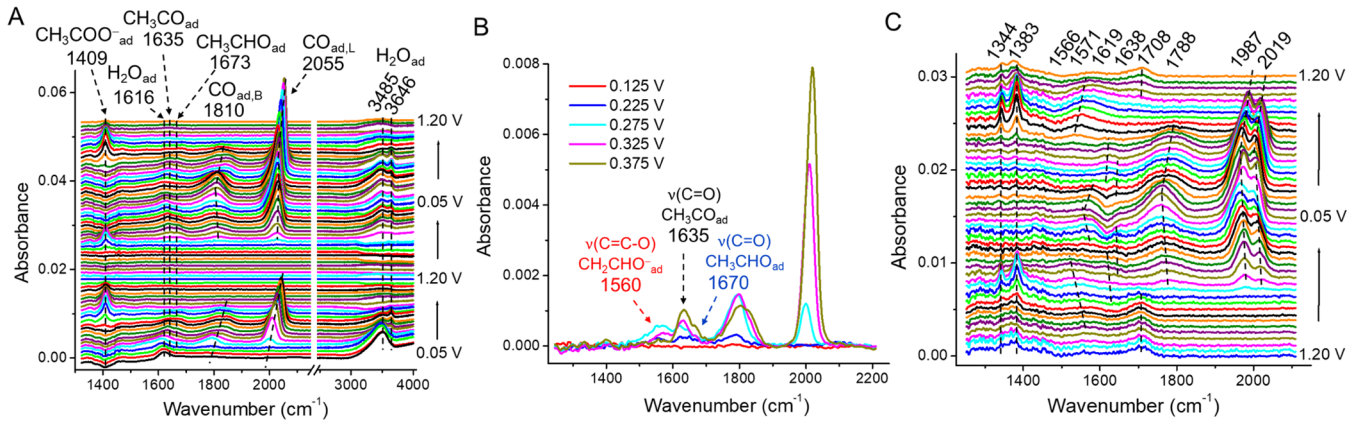

Figure 2. (A, B) SEIRA spectra, simultaneously recorded with DEMS in Figure 1C. In (A), the reference spectrum was taken at 1.2 V. (B) SEIRA spectra in the low-potential region for the first positive-going scan. (C) SEIRA spectra for α-C isotopically labeled ethanol ($CH_3{}^{13}CH_2OH$) oxidation in 0.1 M $CH_3{}^{13}CH_2OH$ + 0.1 M $HClO_4$. In (B) and (C), the reference spectra were taken in background solution (0.1 M $HClO_4$) at each individual potential.

help guide the design of more effective electrocatalysts for DEFCs.

2. RESULTS AND DISCUSSION

Figure 1A shows a schematic illustration of the dual thin-layer spectroelectrochemical flow cell, which allows for the integration of DEMS and SEIRA spectroscopy. The cell has two compartments. In the top compartment, a rough Pt film (~90 nm thick; its AFM image is shown in Figure 1B), chemically deposited on the rectangular face of a hemicylindrical Si prism, was used as the working electrode, while the Si prism served as the infrared window. The infrared light traveled through the Si prism and was then reflected by the Pt film into a liquid N_2-cooled mercury−cadmium−telluride (MCT) detector. An evanescent wave extends into the Pt film and interacts with adsorbates so that a small fraction of the infrared light is absorbed, resulting in a slightly attenuated total reflection. In the bottom compartment, a porous Teflon membrane was used as the interface between vacuum and the aqueous solution. The gases and volatile species, electrochemically generated in the top compartment and transported into the lower compartment, can evaporate into the vacuum, and be subsequently detected with a quadrupole mass spectrometer. The cell details have been described in previous papers.[31,32]

Ethanol electrooxidation on the Pt film was studied using the above-mentioned integrated spectroscopic setup, and the simultaneously recorded DEMS data and SEIRA spectra for potentiodynamic oxidation of ethanol are presented in Figures 1C,D and 2, respectively. The decomposition/oxidation of ethanol began at ca. 0.2 V and exhibited an oxidative peak at ca. 0.25 V in the first positive-going scan (Figure 1D(a)). This process was accompanied by the accumulation of CO and CH_x ad-species on the Pt surface (Figure 2), suggesting that the C−C bond was split at the Pt surface in the upper hydrogen

https://doi.org/10.1021/jacs.2c13401
J. Am. Chem. Soc. XXXX, XXX, XXX−XXX

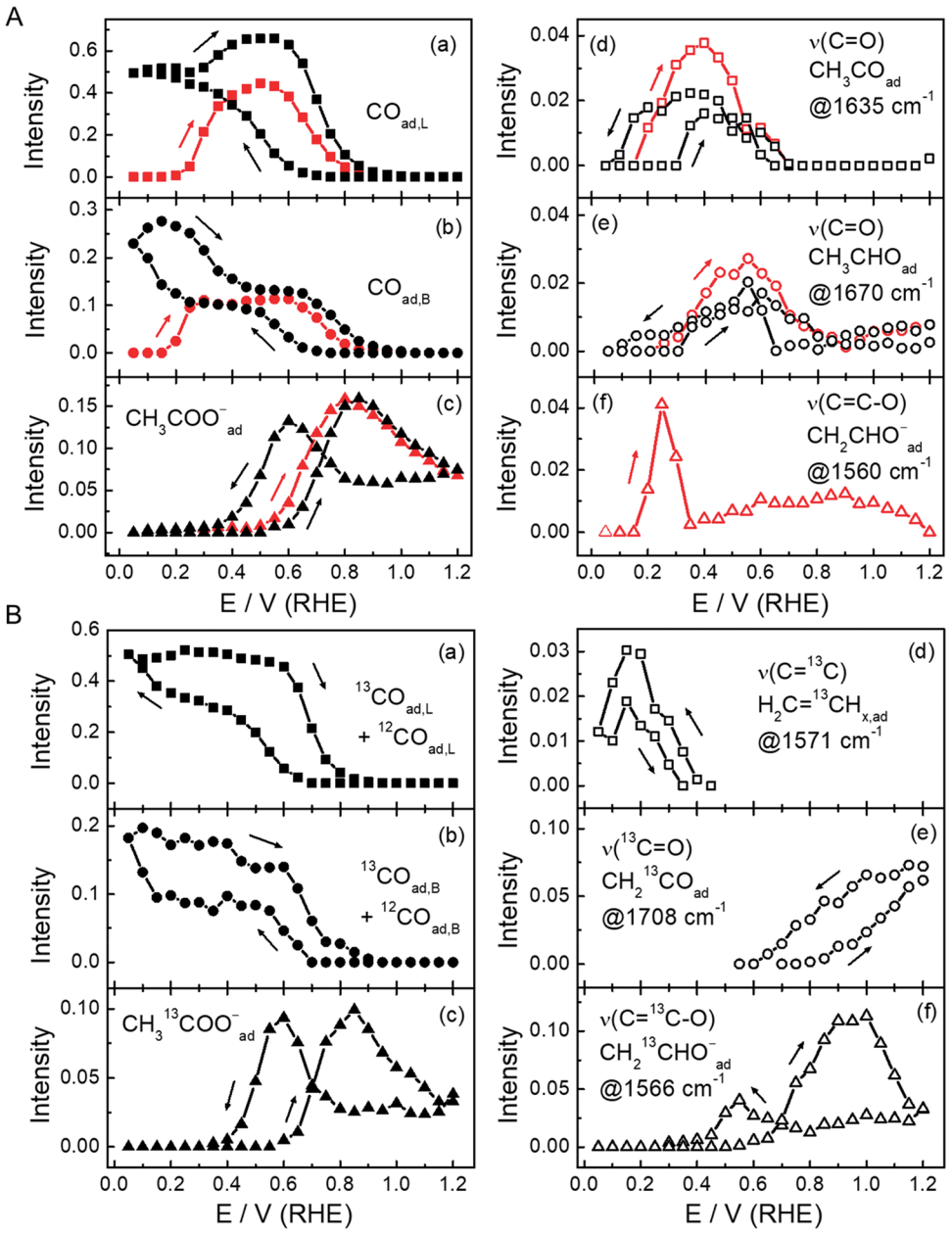

Figure 3. (A) Integrated band intensities for $CO_{ad,L}$ (a) $CO_{ad,B}$ (b), adsorbed acetate (c), acetyl (d), acetaldehyde (e), and enolate (f) plotted vs potential in 0.1 M CH_3CH_2OH. (B) Integrated band intensities for $CO_{ad,L}$ (a) $CO_{ad,B}$ (b), adsorbed acetate (c), vinyl or vinylidene (d), ketene (e), and enolate (f) plotted vs potential in 0.1 M $CH_3{}^{13}CH_2OH$. The red lines indicate the first positive-going scan, while the black lines denote the subsequent negative-going and positive-going scans.

region. The decomposition/oxidation rate of ethanol started to decrease at potentials above 0.25 V since the Pt sites were gradually blocked by CO, CH_x, and $C_2H_xO_y$ ad-species (see below).[13] At potentials just beyond 0.25 V, ethanol decomposition to form adsorbates was slowed down due to a decrease in the number of free Pt surface sites (which have been blocked as stated above), while the oxidation of ethanol to soluble acetaldehyde and acetic acid had not started. Methanol oxidation on Pt also exhibited a similar peak in the first positive-going scan.[33] A fraction of the CH_x ad-species was reductively desorbed to form methane in the hydrogen region so that the mass spectrometric (MS) cyclic voltammogram (MSCV) at m/z = 15 (the fragment of methane, CH_3^+) exhibited a peak at ca. 0.3 V (Figure 1D(b)). This is consistent with the ethanol oxidation on Pt/C nanoparticles and mesoporous Pt catalysts reported by the Pastor group.[25,34] As the potential was scanned beyond 0.5 V, the oxidation of CO and CH_x ad-species started freeing Pt surface sites so that the Faradaic current increased again. The intensities of m/z = 15 (the fragment of acetaldehyde, CH_3^+), m/z = 22 (doubly charged CO_2, CO_2^{2+}), m/z = 29 (the fragment of acetaldehyde, CHO^+), and m/z = 61 (the fragment of ethylacetate, $C_2H_5O_2^+$) also started to increase.[10,25,26] At potentials above 0.9 V, the current decreased due to the formation of platinum oxides that can block the surface. As the potential increased beyond 1.05 V, the current increased again. In the reverse scan, the Faradaic current and mass spectrometric signals at m/z = 22, 29, and 61 started to increase again at potentials below 1.0 V due to the reduction of Pt oxides and generation of fresh Pt surface sites. As the

https://doi.org/10.1021/jacs.2c13401
J. Am. Chem. Soc. XXXX, XXX, XXX−XXX

potential went below 0.8 V, the Faradaic current decreased due to CO_{ad} and $CH_{x,ad}$ poisoning. At potentials below 0.2 V, the MS signals at m/z = 15 and 30 increased, indicating that methane and ethane were generated from the reductive removal of adsorbed CH_x and $C_2H_x(O_y)$ (likely vinyl/vinylidene) (see Figures 2 and 3).[10,17,22,24] It should be noted that the MS signal at m/z = 30 in the high-potential region was mainly due to an isotopic effect from acetaldehyde ($^{13}CHO^+$, CDO^+, and $CH^{17}O^+$) and CO_2 ($C^{18}O^+$).[10] In general, the MS signal of acetaldehyde followed the Faradaic current of ethanol oxidation since acetaldehyde is a major product of ethanol oxidation on Pt (see Table S1).

While acetic acid is not sufficiently volatile to be detected by DEMS, ethylacetate, the product from the reaction between ethanol and acetic acid, was detected, suggesting (albeit indirectly) that acetic acid was also formed. It should be noted that ethylacetate was probably formed directly at the Pt surface rather than in the solution, similar to the formation of methylformate during methanol oxidation.[35] Adsorbed acetate was also detected by SEIRA spectroscopy (Figure 2), again indicating that acetic acid was formed. In 0.1 M ethanol solution, the average CEs for CO_2 and acetaldehyde generation were ca. 4 and 90%, respectively (Table S1). At the peak potential of 0.9 V and the upper potential limit of 1.2 V, the CEs for acetaldehyde were ca. 90 and 63%, respectively. This suggests that at 1.2 V, acetaldehyde can be further oxidized to acetic acid. This is further confirmed by the fact that acetaldehyde can be easily oxidized to acetic acid at 1.2 V (Figure S1). As the concentration of ethanol was decreased to 0.02 M, the CE for acetaldehyde generation decreased, while the CEs for CO_2 and acetic acid increased. This is attributed to the fact that acetaldehyde has a higher probability of being further oxidized to CO_2 and acetic acid at low ethanol concentrations.

To determine from which carbon CO_2 was formed, the oxidation of α-C labeled ethanol was studied (Figure S2). Figure S2 presents the cyclic voltammogram (CV) of $CH_3{}^{13}CH_2OH$ oxidation on a Pt film (a), and the corresponding MSCVs of CO_2 at m/z = 22 ($CO_2{}^{2+}$) and $^{13}CO_2$ at m/z = 22.5 ($^{13}CO_2{}^{2+}$) (b), and $CH_3{}^{13}CHO$ at m/z = 30 ($^{13}CHO^+$) (c). Clearly, CO_2 formation came from both carbon atoms,[17,24] and their ratio was close to one in a single potential cycle between 0.05 and 1.2 V.

In Figure 2, the infrared band, observed at ca. 1409 cm^{-1}, is assigned to the symmetrical stretching vibration of OCO (ν_s(OCO)) from adsorbed acetate since this band was also observed in acetic acid solution (Figure S3).[13] The infrared bands at around 2055 and 1810 cm^{-1} are assigned to ν(C≡O) of linearly bonded CO ($CO_{ad,L}$) and bridge-bonded CO ($CO_{ad,B}$), respectively (Figure 2A).[13,14] They appeared at potentials higher than 0.2 V, suggesting that ethanol can decompose to form adsorbed CO on Pt through C−C bond rupture. The bands at around 3485 and 1616 cm^{-1} are assigned to ν(OH) and the bending mode of HOH [δ(HOH)] for H_2O adsorbed on H-covered Pt, respectively. As the CO band appeared, another band was observed at ca. 3646 cm^{-1}. This band is assigned to ν(OH) for H_2O adsorbed on the top of adsorbed CO.[36] The band at 1635 cm^{-1} is often assigned to acetyl (CH_3CO).[13,14] For only CO adsorbed on Pt, we also observed this band (Figure S4), and thus it can be assigned to ν(C═O) of adsorbed acetyl (major) and also δ(HOH) of H_2O adsorbed on top of the CO adlayer (minor). When isotopically labeled ethanol ($CH_3{}^{13}CH_2OH$) was used, this acetyl band was shifted to 1619 cm^{-1} (Figure 2C). When the reference spectra were taken in background solution (0.1 M $HClO_4$) at each individual potential, two additional bands were clearly observed at ca. 1560 and 1670 cm^{-1} in the low-potential region (Figure 2B), which can be assigned to ν(C═C−O) for adsorbed enolate[37,38] and ν(C═O) for adsorbed acetaldehyde,[39] respectively.

In $CH_3{}^{13}CH_2OH$ solution (Figure 2C), two $CO_{ad,L}$ bands, observed at ca. 1987 and 2019 cm^{-1}, are assigned to $^{13}CO_{ad,L}$ and $^{12}CO_{ad,L}$, respectively. Although there was an intensity transfer from $^{13}CO_{ad,L}$ to $^{12}CO_{ad,L}$ due to their dipole−dipole coupling, the band intensity of $^{13}CO_{ad,L}$ was still higher than that of $^{12}CO_{ad,L}$, suggesting that the CH_2OH group is more easily decomposed into CO than the CH_3 group. The $^{13}CO_{ad,B}$ band shifted to a lower wavenumber (1788 cm^{-1}) (Figure 2C), compared to $^{12}CO_{ad,B}$ (Figure 2A). Two bands, which appeared at 1383 and 1344 cm^{-1}, are assigned to the symmetric stretching $\nu_s(O^{13}CO)$ and asymmetric bending $\delta(CH_3)$ of adsorbed $CH_3{}^{13}COO^-$, respectively. The band at 1535−1575 cm^{-1} is assigned to the ν(C═^{13}C−O) of adsorbed enolate ($CH_2{}^{13}CHO^-$) with a large Stark tuning rate of ca. 113 cm^{-1}/V. The band at around 1708 cm^{-1} is assigned to the $\nu(^{13}C{=}O)$ of adsorbed ketene ($CH_2{}^{13}CO$),[40] which had a Stark tuning rate of 21 cm^{-1}/V. Another band at ca. 1571 cm^{-1} was observed in the hydrogen region with a stark tuning rate of 81 cm^{-1}/V, which could be assigned to the ν(C═^{13}C) of vinyl or vinylidene ad-species ($H_2C{=}{}^{13}CH_{ad}$ or $H_2C{=}{}^{13}C_{ad}$).[41] Feliu et al. previously reported an infrared band occurring in the same wavenumber region for ethylene adsorbed on Pt.[41]

The integrated intensities of infrared bands are plotted vs potential in Figure 3. The $CO_{ad,L}$ and $CO_{ad,B}$ bands onset at ca. 0.2 V, and their intensities increased with increasing potential and then decreased at potentials beyond 0.5 V due to oxidative removal of CO_{ad}. As the CO_{ad} started to be oxidized, the acetate band intensity increased (Figure 3A). It reached a maximum at ca. 0.8 V and then decreased with further increasing potential due to the formation of Pt oxides. In the reverse scan, the intensity of the acetate band increased again at potentials below 0.8 V, reached a maximum at ca. 0.6 V, and then decreased due to displacement by adsorbed CO, CH_x, and $C_2H_x(O_y)$. In the first positive-going scan, the enolate band had a maximum intensity at ca. 0.25 V (Figure 3A(f)), which was parallel to the oxidation peak in Figure 1D(a). This suggests that in the low-potential region, ethanol is preferentially oxidized to enolate on fresh Pt surfaces due to the lack of OH ad-species. Acetyl and acetaldehyde bands also appeared with the enolate band, indicating that ethanol was likely first oxidized to acetaldehyde and then to enolate and acetyl. Adsorbed enolate was subsequently decomposed to form adsorbed CO and CH_x at potentials higher than 0.2 V. Here, adsorbed enolate is proposed to be the precursor for the rupture of the C−C bond to form adsorbed CO and CH_x since the growth rate of the $CO_{ad,L}$ band intensity was proportional to the band intensity of adsorbed enolate (Figures 3A(f) and S5). Recently, Feliu et al. reported that adsorbed OH promoted ethanol adsorption and successive conversion into ethoxy and then $COCH_2$, which was proposed to be the precursor for C−C bond rupture.[42] In this work, ketene ($COCH_2$) ad-species was identified using SEIRA spectroscopy. However, it was formed only at potentials more positive than 0.9 V (Figure 3) from further oxidation of adsorbed enolate. The formation of adsorbed OH is favored on low-coordinated Pt sites,[43] as are the adsorption and decomposition of

https://doi.org/10.1021/jacs.2c13401
J. Am. Chem. Soc. XXXX, XXX, XXX−XXX

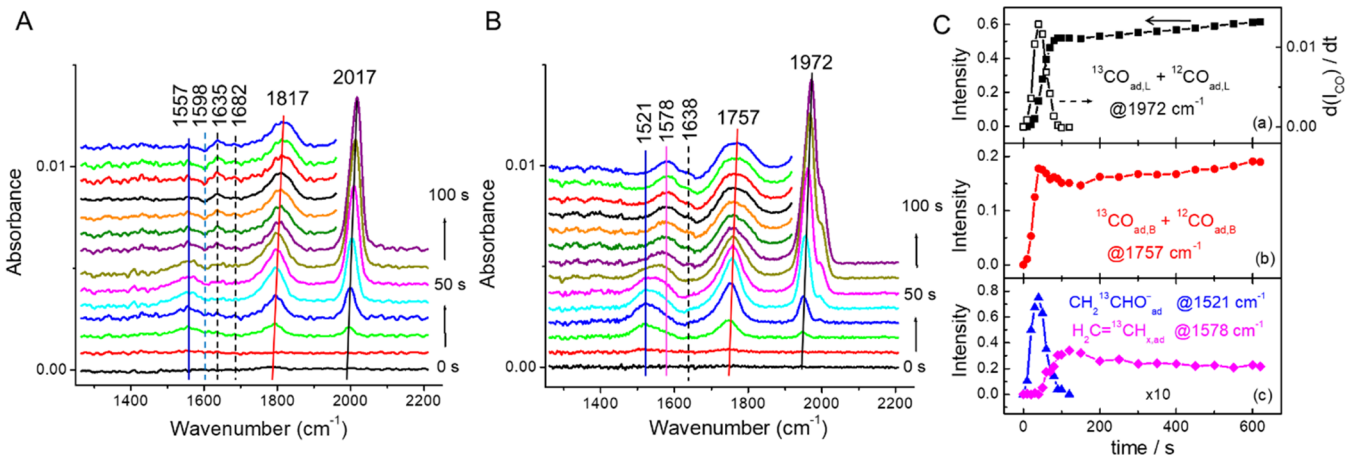

Figure 4. (A, B) Time-dependent SEIRA spectra for ethanol decomposition on a Pt film in 0.1 M CH_3CH_2OH + 0.1 M $HClO_4$ (A) and 0.1 M $CH_3{}^{13}CH_2OH$ + 0.1 M $HClO_4$ (B) at a potential of 0.25 V (vs RHE). (C) Integrated band intensities of $CO_{ad,L}$ (a), $CO_{ad,B}$ (b), and adsorbed enolate and vinyl/vinylidene (c) from (B) plotted vs time. The open symbols in (C, a) represent the derivative of the $CO_{ad,L}$ band intensity with respect to time.

methanol and ethanol. We believe that adsorbed OH might not be necessarily required for the decomposition of ethanol on Pt in electrochemical environments and that ethanol is first oxidized to acetaldehyde then enolate or acetyl, without adsorbed OH. It has been previously reported that acetaldehyde can decompose to form CO_{ad} at 0.05 V (Figure S1),[13,23,39] where OH ad-species are not supposed to form. Ethoxy might be formed from the decomposition of ethanol on Pt in vacuum and has been identified using FTIR spectroscopy.[44] However, we did not observe it during the electrochemical oxidation of ethanol on Pt using SEIRA spectroscopy.

Adsorbed CO and CH_x were further oxidized to CO_2 at potentials higher than 0.5 V. Adsorbed acetyl was then oxidized to acetic acid/acetate at potentials higher than 0.4 V, as indicated by the fact that the increase in the band intensity of adsorbed acetate was parallel to the decrease in the band intensity of adsorbed acetyl with increasing potentials from 0.4 to 0.85 V. In the subsequent negative-going scan, adsorbed enolate was reduced to form vinyl/vinylidene ad-species at potentials below 0.4 V (Figure 3B(d)) and then further reduced to ethane at potentials below 0.1 V. CH_x can also be reduced to form methane at potentials below 0.2 V. This is evidenced by the fact that methane and ethane were observed in the hydrogen region using DEMS during ethanol oxidation (Figure 1) and also the reductive stripping of ethanol adsorbates (see below).[10,17,22−24]

In $CH_3{}^{13}CH_2OH$ solution, the band intensities of $CO_{ad,L}$, $CO_{ad,B}$ and adsorbed acetate plotted vs potential exhibited similar profiles to those in CH_3CH_2OH solution (Figure 3). The band intensity of adsorbed isotopic enolate exhibited a similar potential-dependent profile to adsorbed acetate. The bands of adsorbed isotopic acetyl and acetaldehyde overlapped with δ(HOH) of H_2O_{ad}, so it is difficult to clearly analyze their intensities. The band intensity for adsorbed isotopic ketene at 1708 cm^{-1} increased with increasing potential from 0.85 to 1.2 V, and its increase and the simultaneous decrease in isotopic enolate band intensity suggested that adsorbed enolate was further oxidized to adsorbed ketene.

SEIRA spectra and plots of integrated band intensity vs time for time-dependent ethanol decomposition on Pt at different potentials are presented in Figures 4, S6, S7, and S8. The $CO_{ad,L}$ and $CO_{ad,B}$ bands for ethanol adsorption at 0.25 V were observed at 2017 and 1817 cm^{-1}, and their intensities increased with time: initially fast, and then slowly after ca. 100 s due to the blockage of the surface by adsorbed CO, CH_x and $C_2H_x(O_y)$. The $CO_{ad,L}$ and $CO_{ad,B}$ bands for ethanol adsorption at 0.3 and 0.4 V (Figures S7 and S8) had similar time-dependent profiles. At potentials of 0.25 and 0.3 V, the enolate band, observed at 1557 cm^{-1}, exhibited a maximum intensity at 40 and 25 s, respectively. Its intensity then decreased with time due to the surface blockage by adsorbed CO, CH_x, and $C_2H_x(O_y)$. The derivative of the $CO_{ad,L}$ band intensity with respect to time (open symbols in Figures 4C(a) and S6(a)) exhibited a similar profile to the plot of enolate intensity vs time (Figures 4C(c) and S6(c)). This again suggests that adsorbed enolate is the precursor for C−C bond splitting to form adsorbed CO and CH_x. The intensity of the $CO_{ad,B}$ band reached its maximum much earlier than $CO_{ad,L}$ band since at low CO coverages, CO prefers to occupy the bridge sites. Then, the intensity of the $CO_{ad,B}$ band remained relatively constant, while the intensity of $CO_{ad,L}$ band continued to increase with time. At potentials of 0.25 and 0.3 V, higher CO coverages were obtained, compared to 0.4 V (Figures 4, S7, and S8), likely due to reductive removal of CH_x and $C_2H_x(O)_y$. During ethanol decomposition, a downward band at 1598 cm^{-1} and an upward band at 1635 cm^{-1} developed, which are ascribed to the depletion of adsorbed water and the acetyl adsorption, respectively. A weak band of adsorbed acetaldehyde appeared at ca. 1682 cm^{-1}, which overlapped with the acetyl band at 1635 cm^{-1}.[39]

In $CH_3{}^{13}CH_2OH$ solution (Figures 4B and S9) and at 0.25 V, we observed an infrared peak at 1972 cm^{-1} and a shoulder on the high-frequency side, assigned to $^{13}CO_{ad,L}$ and $^{12}CO_{ad,L}$, respectively. The $^{13}CO_{ad,L}$ band was ca. 45 cm^{-1} red-shifted compared to $^{12}CO_{ad,L}$. The band intensity of $^{13}CO_{ad,L}$ was much stronger than that of $^{12}CO_{ad,L}$, suggesting that the $^{13}CH_2OH$ group is easier to convert into CO_{ad} than the $^{12}CH_3$ group. The $^{13}CO_{ad,B}$ band at ca. 1757 was 60 cm^{-1} red-shifted compared to $^{12}CO_{ad,B}$. The $^{12}CO_{ad,B}$ band overlapped with $^{13}CO_{ad,B}$ so that they were ill-resolved, resulting in a broader $CO_{ad,B}$ band. The band of adsorbed α-C labeled enolate shifted from 1557 to 1521 cm^{-1}, and its intensity also increased compared to unlabeled enolate. The intensification of $CH_2{}^{13}CHO_{ad}{}^-$ band is attributed to an increase in the dipole

https://doi.org/10.1021/jacs.2c13401
J. Am. Chem. Soc. XXXX, XXX, XXX−XXX

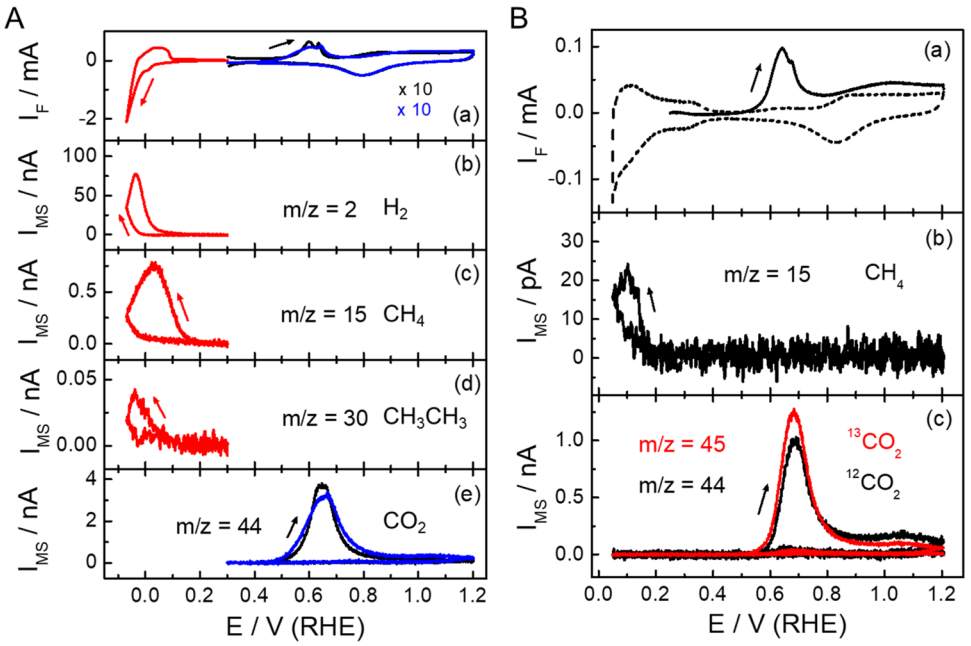

Figure 5. (A) CVs (a) and corresponding MSCVs of H_2 at m/z = 2 (b), methane at m/z = 15 (c), ethane at m/z = 30 (d), and CO_2 at m/z = 44 (e) for reductive and oxidative stripping of adsorbed ethanol adsorbates in 0.1 M $HClO_4$. The adsorbates were formed at 0.3 V in 0.1 M CH_3CH_2OH + 0.1 M $HClO_4$ for about 7 min. Red lines indicate the reductive stripping of ethanol adsorbates, while black lines denote the subsequent oxidative stripping of ethanol adsorbates. Blue lines represent the oxidative stripping of ethanol adsorbates directly. (B) CVs (a) and corresponding MSCVs of CH_4 at m/z = 15 (b), and CO_2 at m/z = 45 and 44 (c) for oxidative stripping and successive negative stripping of adsorbed isotopic ethanol adsorbates in 0.1 M $HClO_4$. The adsorbed isotopic adsorbates were formed at 0.25 V in 0.1 M $CH_3{}^{13}CH_2OH$ + 0.1 M $HClO_4$ for about 10 min. Scan rate: 5 mV/s.

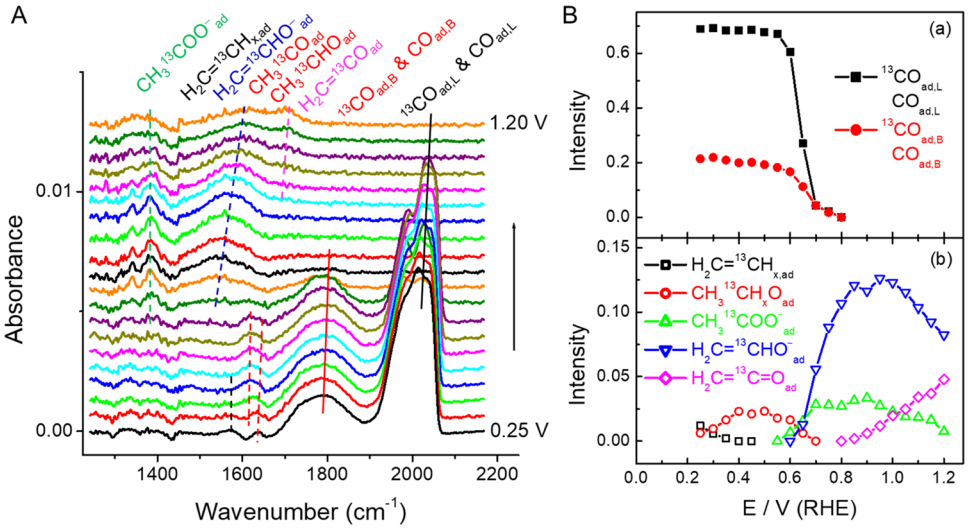

Figure 6. (A) SEIRA spectra for $CH_3{}^{13}CH_2OH$ adsorbate stripping from the Pt film in the positive-going scan in 0.1 M $HClO_4$. The reference spectrum was taken at 0.25 V in 0.1 M $HClO_4$. Scan rate: 5 mV/s. (B) Integrated band intensities of $CO_{ad,L}$ (including $^{13}CO_{ad,L}$ and $^{12}CO_{ad,L}$), $CO_{ad,B}$ (including $^{13}CO_{ad,B}$ and $^{12}CO_{ad,B}$) (a), adsorbed vinyl/vinylidene (H_2C = $^{13}CH_{x,ad}$), acetaldehyde/acetyl ($CH_3{}^{13}CHO_{ad}$/$CH_3{}^{13}CO_{ad}$), acetate ($CH_3{}^{13}COO_{ad}{}^-$), enolate (H_2C = $^{13}CHO_{ad}{}^-$), and ketene (H_2C = $^{13}C{=}O_{ad}$) (b) plotted vs potential.

moment of the C═^{13}C−O bond. Using $CH_3{}^{13}CH_2OH$, another band, which appeared at 1578 cm^{-1}, is assigned to ν(C═^{13}C) of adsorbed vinyl/vinylidene ($CH_2{=}{}^{13}CH_{x,ad}$). In the CH_3CH_2OH solution, the ν(C═C) band of adsorbed vinyl/vinylidene was likely too weak and overlapped with water bending bands so that it was not observed.

The profiles of the integrated band intensities of $CO_{ad,L}$, $CO_{ad,B}$, and adsorbed enolate plotted vs time in $CH_3{}^{13}CH_2OH$ solution are similar to those in CH_3CH_2OH solution (Figures 4C and S9B). The band intensity of adsorbed vinyl/vinylidene initially increased with time and then decreased gradually about 100 s later. After 100 s, the slow decrease in the band intensity of adsorbed vinyl/vinylidene was accompanied by the slow increase in the band intensity of $CO_{ad,L}$, suggesting that adsorbed vinyl/vinylidene was slowly decomposed to adsorbed CO and CH_x.[24]

Besides CO_{ad}, enolate, acetyl, acetaldehyde, vinyl/vinylidene, and ketene ad-species, CH_x ad-species were also formed on Pt. However, they could not be identified with SEIRA spectroscopy. They are likely infrared-inactive according to the surface

https://doi.org/10.1021/jacs.2c13401
J. Am. Chem. Soc. XXXX, XXX, XXX−XXX

Scheme 1. Pathways of Ethanol Oxidation on Pt

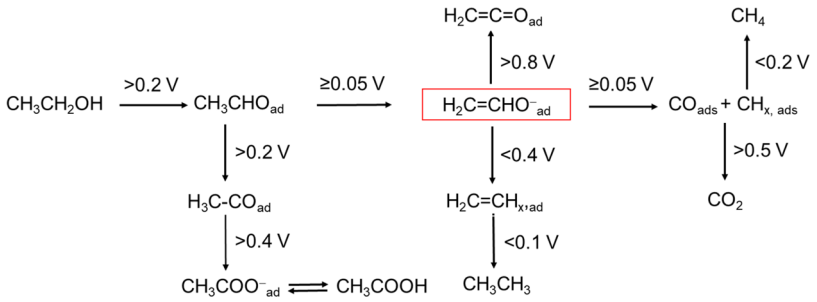

selection rules.[13,14] In contrast, as a complementary technique, DEMS could provide additional information about ethanol adsorbates through their reductive and/or oxidative stripping/desorption.[17,22−24] Figures 5 and S10 present the DEMS data for the reductive and/or oxidative stripping of ethanol adsorbates from a Pt film. After ethanol adsorption and exchanging to an ethanol-free electrolyte, as the potential was first scanned negatively down to −0.05 V, a large amount of methane and a small amount of ethane were detected, suggesting that adsorbed CH_x and $C_2H_x(O_y)$ were formed during ethanol decomposition.[10,17,22−24] In Figure 5B, the total amounts of $^{13}CO_2$ and $^{12}CO_2$ from oxidative stripping of adsorbates were comparable. For the first CO_2 peak at 0.65 V, the amount of $^{13}CO_2$ is relatively higher than $^{12}CO_2$. In contrast, in the second CO_2 peak at 1.05 V, the amount of $^{12}CO_2$ is relatively higher than $^{13}CO_2$. The first CO_2 peak is ascribed to the oxidation of $^{13}CO_{ad}$ and $^{12}CO_{ad}$, while the second CO_2 peak is attributed to the oxidation of $^{12}CH_{x,ad}$ and $^{12}CH_2{}^{13}CH_x(O_y)_{ad}$, which are more difficult to be oxidized. In the subsequent negative-going scan, small amounts of methane were still formed in the hydrogen region. This is consistent with the previous findings for the electrooxidation of isotopically labeled ethanol on polycrystalline Pt and porous Pt films.[17,24]

During the oxidative stripping of $CH_3{}^{13}CH_2OH$ adsorbates that were formed at 0.25 and 0.3 V, the SEIRA spectra were simultaneously recorded and are shown in Figures 6 and S11, respectively. Upon ethanol adsorption at 0.25 and 0.3 V, large amounts of CO_{ad} were formed, while small amounts of adsorbed vinyl/vinylidene, acetaldehyde, and acetyl were also formed on Pt. CO_{ad} started to be oxidized as the potential went up to ca. 0.5 V and was completely removed from Pt at potentials >0.8 V. With increasing potential, the band intensity of adsorbed vinyl/vinylidene and acetaldehyde decreased, while the band intensity of adsorbed acetyl increased and reached a maximum at 0.4−0.5 V. It should be noted that the integrated band intensities of both adsorbed acetyl and acetaldehyde are shown in Figures 6B and S11B since they significantly overlapped. Afterward, the band intensity of adsorbed acetyl decreased with further increasing potential, while the band intensity of adsorbed enolate and acetate increased. As the potential went up beyond 0.85 V, the band intensity of adsorbed ketene started to increase, while the band intensity of adsorbed enolate decreased, suggesting that enolate was gradually oxidized to adsorbed ketene. A portion of the adsorbed enolate was also oxidized into CO_2 at potential >0.85 V (Figures 5B(c) and S10C(c)). The band intensity of adsorbed acetate also gradually decreased with increasing potential from 0.9 V, likely due to the displacement of adsorbed acetate by OH/O adsorption.[13,14] It is evident that C-2 ad-species were gradually oxidized from adsorbed vinyl/vinylidene and adsorbed acetaldehyde through adsorbed acetyl and then adsorbed enolate into adsorbed ketene without C−C bond rupture, while a portion of adsorbed enolate was also oxidized to CO_2 with C−C bond splitting. Small amounts of acetic acid were also formed during the positive stripping of ethanol adsorbates at high potentials, as indicated by the decrease of the band intensity of adsorbed acetate at potentials >0.9 V (Figures 6 and S11).

Based on our experimental data, the mechanism of ethanol oxidation on Pt can be described by Scheme 1. Ethanol electrooxidation on Pt in acidic media proceeds through many parallel and successive pathways. In one pathway, ethanol is oxidized to acetaldehyde, which can be further oxidized to acetic acid through acetyl ad-species by OH ad-species. In another parallel pathway, acetaldehyde was dehydrated to form adsorbed enolate, which can dissociate into CO and CH_x ad-species through C−C bond splitting, or be oxidized to ketene at high potentials or reduced to vinyl/vinylidene ad-species in the hydrogen region. Acetaldehyde is the major product without C−C bond rupture, while CO_2 is only a minor product due to slower C−C bond rupture and successive oxidation than the formation of acetaldehyde without C−C bond splitting. Thus, increasing the CO_2 efficiency will require the design of more effective electrocatalysts to enhance the C−C bond rupture of adsorbed enolate for ethanol oxidation.

3. CONCLUSIONS

We have built a spectroscopic platform, which combined SEIRA spectroscopy and DEMS, to study ethanol and isotopically labeled ethanol decomposition/oxidation on a Pt film electrode under well-defined electrolyte flow conditions. $CO_{ad,L}$, $CO_{ad,B}$, acetate, acetaldehyde, acetyl, enolate, ketene, and vinyl/vinylidene were identified with SEIRA spectroscopy as ad-species. In particular, adsorbed enolate, ketene, and vinyl/vinylidene were identified for the first time with SEIRA spectroscopy and adsorbed enolate was proposed to be the precursor for C−C bond splitting during ethanol electrooxidation. CH_x ad-species were also formed on Pt but were infrared-inactive. However, they can be detected as methane with DEMS through reductive stripping. Ethanol is first oxidized to acetaldehyde at potentials above 0.2 V, which can be further oxidized to enolate by the removal of one β-H. The enolate is further decomposed to form CO_{ad} and $CH_{x,ad}$ through C−C bond rupture or further oxidized to ketene without C−C splitting. Meanwhile, acetaldehyde can also be oxidized to acetic acid through adsorbed acetyl by the removal of an α-H and addition of an OH at potentials above 0.4 V, and acetic acid cannot be further oxidized at room temperature. Adsorbed enolate can also be reduced to form vinyl/

https://doi.org/10.1021/jacs.2c13401
J. Am. Chem. Soc. XXXX, XXX, XXX−XXX

vinylidene ad-species and then ethane in the hydrogen region. The enolate pathway and the acetate/acetic acid pathway are competing processes, and both are slower than ethanol oxidation to acetaldehyde at potentials below 1.0 V, and thus ethanol oxidation on Pt mainly forms acetaldehyde. To increase the CE of CO_2 generation, it will be necessary to find effective catalysts to enhance the enolate pathway.

■ ASSOCIATED CONTENT

Supporting Information

The Supporting Information is available free of charge at https://pubs.acs.org/doi/10.1021/jacs.2c13401.

Experimental details, additional SEIRA spectra and DEMS data, and a table of infrared band assignment (PDF)

■ AUTHOR INFORMATION

Corresponding Author

Héctor D. Abruña − *Department of Chemistry and Chemical Biology, Baker Laboratory, Cornell University, Ithaca, New York 14853-1301, United States;* orcid.org/0000-0002-3948-356X; Email: hda1@cornell.edu

Author

Hongsen Wang − *Department of Chemistry and Chemical Biology, Baker Laboratory, Cornell University, Ithaca, New York 14853-1301, United States;* orcid.org/0000-0001-7926-2895

Complete contact information is available at: https://pubs.acs.org/10.1021/jacs.2c13401

Notes

The authors declare no competing financial interest.

■ ACKNOWLEDGMENTS

This material is based upon work supported by the Air Force Office of Scientific Research under the MURI: Molecular Level Studies of Solid-Liquid Interfaces in Electrochemical Processes award number FA9550-18-1-0420. This work made use of the Cornell Center for Materials Research Shared Facilities which are supported through the NSF MRSEC program (DMR-1719875).

■ REFERENCES

(1) Jiao, K.; Xuan, J.; Du, Q.; Bao, Z.; Xie, B.; Wang, B.; Zhao, Y.; Fan, L.; Wang, H.; Hou, Z.; Huo, S.; Brandon, N. P.; Yin, Y.; Guiver, M. D. Designing the Next Generation of Proton-Exchange Membrane Fuel Cells. *Nature* **2021**, *595*, 361−369.

(2) Mustain, W. E.; Chatenet, M.; Page, M.; Kim, Y. S. Durability Challenges of Anion Exchange Membrane Fuel Cells. *Energy Environ. Sci.* **2020**, *13*, 2805−2838.

(3) Ramaswamy, N.; Mukerjee, S. Alkaline Anion-Exchange Membrane Fuel Cells: Challenges in Electrocatalysis and Interfacial Charge Transfer. *Chem. Rev.* **2019**, *119*, 11945−11979.

(4) Bianchini, C.; Shen, P. K. Palladium-Based Electrocatalysts for Alcohol Oxidation in Half Cells and in Direct Alcohol Fuel Cells. *Chem. Rev.* **2009**, *109*, 4183−4206.

(5) Chang, J.; Wang, G.; Wang, M.; Wang, Q.; Li, B.; Zhou, H.; Zhu, Y.; Zhang, W.; Omer, M.; Orlovskaya, N.; Ma, Q.; Gu, M.; Feng, Z.; Wang, G.; Yang, Y. Improving Pd−N−C Fuel Cell Electrocatalysts through Fluorination-Driven Rearrangements of Local Coordination Environment. *Nat. Energy* **2021**, *6*, 1144−1153.

(6) Badwal, S. P. S.; Giddey, S.; Kulkarni, A.; Goel, J.; Basu, S. Direct Ethanol Fuel Cells for Transport and Stationary Applications − A Comprehensive Review. *Appl. Energy* **2015**, *145*, 80−103.

(7) Xu, H.; Rebollar, D.; He, H.; Chong, L.; Liu, Y.; Liu, C.; Sun, C.-J.; Li, T.; Muntean, J. V.; Winans, R. E.; Liu, D.-J.; Xu, T. Highly Selective Electrocatalytic CO_2 Reduction to Ethanol by Metallic Clusters Dynamically Formed from Atomically Dispersed Copper. *Nat. Energy* **2020**, *5*, 623−632.

(8) Wang, P.; Yang, H.; Tang, C.; Wu, Y.; Zheng, Y.; Cheng, T.; Davey, K.; Huang, X.; Qiao, S.-Z. Boosting Electrocatalytic CO_2−to−Ethanol Production via Asymmetric C−C Coupling. *Nat. Commun.* **2022**, *13*, No. 3754.

(9) Nguyen, T. N.; Guo, J.; Sachindran, A.; Li, F.; Seifitokaldani, A.; Dinh, C.-T. Electrochemical CO_2 Reduction to Ethanol: from Mechanistic Understanding to Catalyst Design. *J. Mater. Chem. A* **2021**, *9*, 12474−12494.

(10) Wang, H.; Jusys, Z.; Behm, R. J. Ethanol Electrooxidation on a Carbon-Supported Pt Catalyst: Reaction Kinetics and Product Yields. *J. Phys. Chem. B* **2004**, *108*, 19413−19424.

(11) Bach Delpeuch, A.; Chatenet, M.; Rau, M. S.; Cremers, C. Influence of H- and OH-Adsorbates on the Ethanol Oxidation Reaction − a DEMS Study. *Phys. Chem. Chem. Phys.* **2015**, *17*, 10881−10893.

(12) Kutz, R. B.; Braunschweig, B.; Mukherjee, P.; Behrens, R. L.; Dlott, D. D.; Wieckowski, A. Reaction Pathways of Ethanol Electrooxidation on Polycrystalline Platinum Catalysts in Acidic Electrolytes. *J. Catal.* **2011**, *278*, 181−188.

(13) Heinen, M.; Jusys, Z.; Behm, R. J. Ethanol, Acetaldehyde and Acetic Acid Adsorption/Electrooxidation on a Pt Thin Film Electrode under Continuous Electrolyte Flow: An in situ ATR-FTIRS Flow Cell Study. *J. Phys. Chem. C* **2010**, *114*, 9850−9864.

(14) Shao, M. H.; Adzic, R. R. Electrooxidation of Ethanol on a Pt Electrode in Acid Solutions: in situ ATR-SEIRAS Study. *Electrochim. Acta* **2005**, *50*, 2415−2422.

(15) Mostafa, E.; Abd-El-Latif, A.-E.-A. A.; Ilsley, R.; Attardd, G.; Baltruschat, H. Quantitative DEMS Study of Ethanol Oxidation: Effect of Surface Structure and Sn Surface Modification. *Phys. Chem. Chem. Phys.* **2012**, *14*, 16115−16129.

(16) Leung, L. W. H.; Chang, S. C.; Weaver, M. J. Real-time FTIR Spectroscopy as an Electrochemical Mechanistic Probe: Electro-oxidation of Ethanol and Related Species on Well-Defined Pt(111) Surface. *J. Electroanal. Chem.* **1989**, *266*, 317−336.

(17) Iwasita, T.; Pastor, E. A DEMS and FTIR Spectroscopic Investigation of Adsorbed Ethanol on Polycrystalline Platinum. *Electrochim. Acta* **1994**, *39*, 531−537.

(18) Willsau, J.; Heitbaum, J. Elementary Steps of Ethanol Oxidation on Pt in Sulfuric Acid as Evidenced by Isotope Labelling. *J. Electroanal. Chem.* **1985**, *194*, 27−35.

(19) Lai, S. C. S.; Kleyn, S. E. F.; Rosca, V.; Koper, M. T. M. Mechanism of the Dissociation and Electrooxidation of Ethanol and Acetaldehyde on Platinum as Studied by SERS. *J. Phys. Chem. C* **2008**, *112*, 19080−19087.

(20) Souza-Garcia, J.; Herrero, E.; Feliu, J. M. Breaking the C−C Bond in the Ethanol Oxidation Reaction on Platinum Electrodes: Effect of Steps and Ruthenium Adatoms. *ChemPhysChem* **2010**, *11*, 1391−1394.

(21) Wang, H.-F.; Liu, Z.-P. Comprehensive Mechanism and Structure-Sensitivity of Ethanol Oxidation on Platinum: New Transition-State Searching Method for Resolving the Complex Reaction Network. *J. Am. Chem. Soc.* **2008**, *130*, 10996−11004.

(22) Bittins-Cattaneo, B.; Wilhelm, S.; Cattaneo, E.; Buschmann, H. W.; Vielstich, W. Intermediates and Products of Ethanol Oxidation on Platinum in Acid Solution. *Ber. Bunsenges. Phys. Chem.* **1988**, *92*, 1210−1218.

(23) Wang, H.; Jusys, Z.; Behm, R. J. Ethanol and Acetaldehyde Adsorption on a Carbon-Supported Pt Catalyst: A Comparative DEMS Study. *Fuel Cells* **2004**, *4*, 113−125.

(24) Schmiemann, U.; Müller, U.; Baltruschat, H. The Influence of the Surface Structure on the Adsorption of Ethene, Ethanol and

Cyclohexene as Studied by DEMS. *Electrochim. Acta* **1995**, *40*, 99−107.
(25) Flórez-Montaño, J.; García, G.; Guillén-Villafuerte, O.; Rodríguez, J. L.; Planes, G. A.; Pastor, E. Mechanism of Ethanol Electrooxidation on Mesoporous Pt Electrode in Acidic Medium Studied by a Novel Electrochemical Mass Spectrometry Set-up. *Electrochim. Acta* **2016**, *209*, 121−131.
(26) Wang, H.; Jusys, Z.; Behm, R. J. Ethanol Electro-oxidation on Carbon-Supported Pt, PtRu and Pt_3Sn catalysts: A Quantitative DEMS Study. *J. Power Source* **2006**, *154*, 351−359.
(27) Kowal, A.; Li, M.; Shao, M.; Sasaki, K.; Vukmirovic, M. B.; Zhang, J.; Marinkovic, N. S.; Liu, P.; Frenkel, A. I.; Adzic, R. R. Ternary $Pt/Rh/SnO_2$ Electrocatalysts for Oxidizing Ethanol to CO_2. *Nat. Mater.* **2009**, *8*, 325−330.
(28) Bach Delpeuch, A.; Maillard, F.; Chatenet, M.; Soudant, P.; Cremers, C. Ethanol Oxidation Reaction (EOR) Investigation on Pt/C, Rh/C, and Pt-Based Bi- and Tri-Metallic Electrocatalysts: A DEMS and in situ FTIR Study. *Appl. Catal. B: Environ.* **2016**, *181*, 672−680.
(29) Wang, H.; Abruña, H. D. Electrocatalysis of Direct Alcohol Fuel Cells: Quantitative DEMS Studies. *Struct. Bonding* **2011**, *141*, 33−83.
(30) Piwowar, J.; Lewera, A. On the Absence of a Beneficial Role of Rh towards C−C bond Cleavage during Low Temperature Ethanol Electrooxidation on PtRh Nanoalloys. *J. Electroanal. Chem.* **2020**, *875*, No. 114229.
(31) Wang, H.; Abruña, H. D. New Insights into Methanol and Formic Acid Electro-Oxidation on Pt: Simultaneous DEMS and ATR-SEIRAS Study under Well-Defined Flow Conditions and Simulations of CO Spectra. *J. Chem. Phys.* **2022**, *156*, No. 034703.
(32) Heinen, M.; Chen, Y. X.; Jusys, Z.; Behm, R. J. In Situ ATR-FTIRS Coupled with On-Line DEMS under Controlled Mass Transport Conditions - A Novel Tool for Electrocatalytic Reaction Studies. *Electrochim. Acta* **2007**, *52*, 5634−5643.
(33) Krausa, M.; Vielstich, W. Study of the Electrocatalytic Influence of Pt/Ru and Ru on the Oxidation of Residues of Small Organic Molecules. *J. Electroanal. Chem.* **1994**, *379*, 307−314.
(34) Guillén-Villafuerte, O.; García, G.; Arévalo, M. C.; Rodríguez, J. L.; Pastor, E. New Insights on the Electrochemical Oxidation of Ethanol on Carbon-Supported Pt Electrode by a Novel Electrochemical Mass Spectrometry Configuration. *Electrochem. Commun.* **2016**, *63*, 48−51.
(35) Abd-El-Latif, A. A.; Baltruschat, H. Formation of Methylformate during Methanol Oxidation Revisited: The Mechanism. *J. Electroanal. Chem.* **2011**, *662*, 204−212.
(36) Osawa, M.; Tsushima, M.; Mogami, H.; Samjeské, G.; Yamakata, A. Structure of Water at the Electrified Platinum-Water Interface: A Study by Surface-Enhanced Infrared Absorption Spectroscopy. *J. Phys. Chem. C* **2008**, *112*, 4248−4256.
(37) Zaki, M. I.; Hasan, M. A.; Pasupulety, L. Surface Reactions of Acetone on Al_2O_3, TiO_2, ZrO_2, and CeO_2: IR Spectroscopic Assessment of Impacts of the Surface Acid-Base Properties. *Langmuir* **2001**, *17*, 768−774.
(38) Okanishi, T.; Katayama, Y.; Ito, R.; Muroyama, H.; Matsui, T.; Eguchi, K. Electrochemical Oxidation of 2-Propanol over Platinum and Palladium Electrodes in Alkaline Media Studied by in situ Attenuated Total Reflection Infrared Spectroscopy. *Phys. Chem. Chem. Phys.* **2016**, *18*, 10109−10115.
(39) Ma, X.-Y.; Ding, C.; Li, H.; Jiang, K.; Duan, S.; Cai, W.-B. Revisiting the Acetaldehyde Oxidation Reaction on a Pt Electrode by High-Sensitivity and Wide-Frequency Infrared Spectroscopy. *J. Phys. Chem. Lett.* **2020**, *11*, 8727−8734.
(40) Mitchell, G. E.; Radloff, P. L.; Greenlief, C. M.; Henderson, M. A.; White, J. M. The Surface Chemstry of Ketene on Pt(111) II. HREELS. *Surf. Sci.* **1987**, *183*, 403−426.
(41) Berná, A.; Kuzume, A.; Herrero, E.; Feliu, J. M. Ethylene Adsorption and Oxidation on Pt(h k l) in Acidic Media. *Surf. Sci.* **2008**, *602*, 84−94.
(42) Rizo, R.; Ferre-Vilaplana, A.; Herrero, E.; Feliu, J. M. Ethanol Electro-oxidation Reaction Selectivity on Platinum in Aqueous Media *ACS Sustainable Chem. Eng.* 2022 DOI: 10.1021/acssuschemeng.2c02663.
(43) Rizo, R.; Fernández-Vidal, J.; Hardwick, L. J.; Attard, G. A.; Vidal-Iglesias, F. J.; Climent, V.; Herrero, E.; Feliu, J. M. Investigating the Presence of Adsorbed Species on Pt steps at Low Potentials. *Nat. Commun.* **2022**, *13*, No. 2550.
(44) Raskó, J.; Dömök, M.; Baán, K.; Erdőhelyi, A. FTIR and Mass Spectrometric Study of the Interaction of Ethanol and Ethanol−Water with Oxide-Supported Platinum Catalysts. *Appl. Catal., A* **2006**, *299*, 202−211.

https://doi.org/10.1021/jacs.2c13401
J. Am. Chem. Soc. XXXX, XXX, XXX−XXX